Title: Electric field redistribution during tissue electroporation: its potential impact on treatment planning.

Titre: Redistribution du champ électrique pendant l'électroporation des tissues: son impact potentiel dans la planification des traitements.

Authors: Antoni Ivorra [a,*], Boris Rubinsky [b], Lluis M. Mir [c,d]

[a] Dept. of Information and Communication Technologies, Universitat Pompeu Fabra, Carrer Tanger 122-140, E-08018, Barcelona, Spain
[b] Dept. of Bioengineering, Dept. of Mechanical Engineering and Graduate Program in Biophysics, University of California at Berkeley, Berkeley, CA 94720, USA
[c] CNRS, UMR 8203, Institut Gustave-Roussy, 39 r. C. Desmoulins, F-94805 Villejuif, France
[d] Univ Paris-Sud, UMR 8203

[*] Correspondig author
E-mail address: antoni.ivorra@gmail.com

Abstract:
Electroporation is the phenomenon in which cell membrane permeability is increased by exposing the cell to short high electric field pulses. Electroporation is accompanied by an increase of tissue electrical conductivity during the pulses. Such conductivity increase results in a redistribution of the electric field magnitude that can be simulated with simple functions describing the change in tissue conductivity. Experiments on potato tuber reveal that the conductivity increase phenomenon has indeed a significant impact on field distribution, and validate the use of models that take into account such conductivity alteration. For instance, the error in electroporated area estimation can decrease from 30 % to 3 %.

Résumé:
Electroporation est le phénomène dans lequel la perméabilité de la membrane cellulaire est augmentée en exposant la cellule à des impulsions électriques courtes et de forte intensité. L'électroporation est accompagnée par une augmentation de la conductivité électrique des tissus pendant les impulsions électriques. Une telle augmentation de conductivité provoque une redistribution de l'amplitude du champ électrique qui peut être simulée avec des simple fonctions décrivant le changement de la conductivité tissulaire. Des expériences sur des pommes de terre ont révélé que le phénomène d'augmentation de conductivité a effectivement un impact significatif sur la distribution du champ. Elles ont validé ces modèles qui prennent en compte ce changement de conductivité. Par exemple, une erreur dans l'estimation de la région electroporée de 30% a pu être réduite à 3 %.

Keywords: Electroporation, Electropermeabilization, Tissue Conductivity, Electric Field, Potato, Finite Element Method.

Mots-clés: Electroporation, Electroperméabilisation, Conductivité tissulaire, Champ Electrique, Pomme de terre, Méthode des élements finis.

1. Introduction

Electroporation, or electropermeabilization, is the phenomenon in which cell membrane permeability to ions and macromolecules is increased by exposing the cell to short (microsecond to millisecond) high electric field pulses. Reversible electroporation of living tissues is the basis for different therapeutic maneuvers on clinical use or under study [1] such as the in vivo introduction of genes into cells (electrogenetherapy) [2, 3] and the introduction of anti-cancer drugs into undesirable cells (electrochemotherapy)[4]. More recently, irreversible electroporation (IRE) has also found a use in tissues as a minimally invasive surgical procedure to ablate undesirable tissue without the use of adjuvant agents [5-7].

Electroporation is a dynamic phenomenon that depends on the local transmembrane voltage. It is generally accepted that, for a given pulse duration and shape, a specific transmembrane voltage threshold exists for the manifestation of the electroporation phenomenon (from 0.5 V to 1 V). This leads to the definition of an electric field magnitude threshold for electroporation (E_{rev}); only the cells within areas where the electric field magnitude ($|\mathbf{E}|$) is larger than E_{rev} are electroporated. If a second threshold (E_{irrev}) is reached or surpassed, the electroporation phenomenon will be too intense and cell homeostasis will be altered to the point of compromising cell viability. In addition, a larger threshold can also be defined ($E_{thermal}$) for the manifestation of thermal damage caused by the Joule effect. This is particularly relevant in the case of IRE ablation techniques: if irreversibility threshold is surpassed but thermal threshold is not reached then cells are destroyed but tissue scaffold is spared and that facilitates post-treatment healing [7].

For more than ten years [8-10] researchers have been employing numerical methods (e.g. the Finite Element Method (FEM)) for computing the electric field magnitude distribution and therefore for predicting the tissue volumes that will be effectively electroporated under a certain sample and electrode configuration. Until a few years ago, the models employed for computing the electric field distribution presupposed that the conductivity of tissues was inalterable. And those models were validated empirically with reasonably positive results [11, 12]. However, recently it has been introduced a refinement that is supposed to increase the accuracy of the predictions [13, 14]: the electrical conductivity of a tissue is not constant but depends on the electric field magnitude it is experiencing. This feature models the fact that when electroporation occurs the conductivity of tissues increases abruptly and significantly [15-21]. Such conductivity increase results in a field redistribution which in turn results in a new conductivity redistribution and so on. Hence, when a high-voltage pulse is applied to a tissue, if electroporation occurs, the final electric field distribution will not be reached immediately and such final field distribution will be different from the distribution computed assuming that the tissue conductivity is constant.

Although this new refinement is perfectly reasonable, in our opinion, and to the best of our knowledge, no valid empirical evidence has been provided to support it against the more common and simpler models based on constant conductivities. It is precisely the purpose of the present study to provide evidences in this sense.

Following the replacement concept of the 3 Rs approach for animal testing (reduction of the number of animals, refinement of procedures to reduce distress, and replacement of animal

with non-animal techniques [22]), it is convenient to note that some vegetables can be a proper alternative to animal tissues for studying bioelectrical aspects of tissue electroporation. In particular, raw potato tuber is a good choice because any electroporated area will start to be distinctively darker at about 5 hours after electroporation. This darkening process is very likely due to an accelerated oxidation of chemical constituents caused by a decompartmentalization of certain enzymes and substrates [23, 24] that occurs after intracellular contents release caused by electroporation. We do believe that in most cases darkening indicates complete cell lysis (i.e. irreversible electroporation) but in others, in which darkening is mild, it may be indicating partial and transitory release of intracellular contents due to reversible electroporation (i.e. original cell membrane permeability is restored sometime after the pulses). Further details on this issue are provided in the next sections.

The present study comprises two experimental parts. First, with an electrode setup that produces an uniform electric field distribution, it was measured the electrical conductivity evolution of potato tuber samples during electroporation pulses of different magnitudes. Twelve hours after the electroporation pulses, it was analyzed and modeled how dark the samples had become as a function of the applied electric field. In the second series of experiments, potato slabs were electroporated with needle electrodes in a configuration that resembles those used in electroporation treatments and that produces an electric field distribution that is far from being uniform. The resulting electroporated areas, as assessed by observable darkening, were then compared to the areas predicted by simulations based on the darkening model and the conductivity models extracted from the first series of experiments.

The contents of the present study was partially disclosed in a conference presentation [25]. Here we expand the explanation of some aspects concerning the methods and the results. Furthermore, the present manuscript contains a very significant novelty concerning the proposed simulation methodology that we did not notice at the time of the conference presentation: the simulation results are optimum when the model for the dependence of tissue conductivity on the electric field is extracted from experimental data measured immediately after the cell membrane charging transient that follows the voltage pulse onset.

2. Materials and methods

2.1 Uniform field electroporation

Sixteen potato tuber cylinders of 5 mm in diameter and approximately 5 mm in height were electroporated between two large plate electrodes made of aluminum (Fig 1.a) attached to a dielectric digital caliper (Digimatic by Mitutoyo Corp., Kawasaki, Japan) for accurate assessment of cylinder height. If the sample is homogenous, as it is the case of potato tissue at macroscopic level, this electrode and sample configuration produces a completely uniform electric field magnitude equal to the ratio between the applied voltage and the electrode separation distance.

The electroporation protocol consisted of a single pulse of 400 µs. Multiple voltages, ranging from 50 V to 500V, were selected in the electroporation pulse generator (ECM 830 by BTX-Harvard Apparatus Inc., Holliston, MA, USA).

Voltage and current waveforms were recorded with a digital oscilloscope (WaveRunner 44Xi by LeCroy Corp., Chestnut Ridge, NY, USA), a high voltage probe (ADP305 by LeCory Corp.) and a current probe (AP015 by LeCroy Corp.). From those recordings, instant conductivity values ($\sigma(t)$) were computed as:

$$\sigma(t) = \frac{i(t)}{v(t)} \frac{l}{S} \qquad (1)$$

where $i(t)$ is the measured current, $v(t)$ is the measured voltage, l is the distance between the electrodes (as measured by the digital caliper) and S is the section of the sample (=19.6 mm^2).

After the electroporation pulse, the samples were kept in Petri dishes (for minimizing dehydration) for 12 hours at room temperature. Then a single picture of all the samples on a white sheet was taken with a digital camera (C-7070 by Olympus Corp., Tokyo, Japan). The obtained color image was converted to a grayscale image and brightness and contrast were adjusted (software Photoshop 8.0 by Adobe Systems Inc., Mountain View, CA, USA) so that the white paper had a 0% black content ("K"), the non treated potato cylinder had a K of about 60% and the darkest cylinders ($|\mathbf{E}| > 800$ V/cm) had a K of about 95%. Finally, the black content of the samples was represented against the electric field magnitude each one of them had experienced and a linear piecewise function was obtained for the relationship between K and $|\mathbf{E}|$.

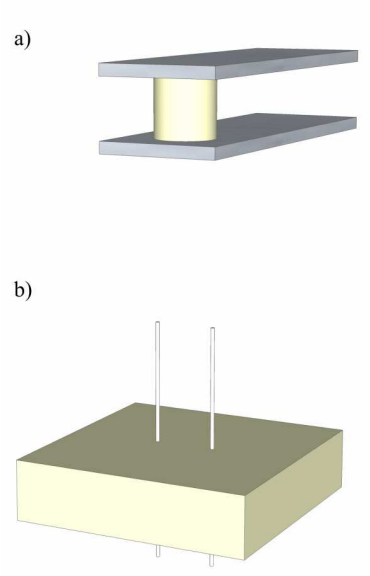

Fig. 1. Representation of the electroporation setups employed in the current study. (a) Uniform field electroporation: potato tuber cylinders of 5 mm in diameter and approximately 5 mm in height are electroporated between two parallel plate electrodes. (b) Ununiform field electroporation: a slab of potato tuber is electroporated with two parallel needles at a 5 mm separation distance.

(Here Fig. 1, single column)

2.2 Ununiform field electroporation

A two needle electroporation array (5 mm separation, 0.3 mm in diameter, model 533 by BTX-Harvard Apparatus Inc., Holliston, MA, USA) was inserted across the center of a rectangular piece (20 mm × 20 mm × 5 mm) of potato tuber (Fig 1.b). Then a single pulse of 400 µs and 300 V was applied with the ECM 830. The same process was repeated with a 500 V pulse.

Both pieces were kept in Petri dishes for 12 hours and pictures were obtained and processed as it is described in the previous subsection (result images are subfigures a and f of Fig 4; only the central 15 mm × 15 mm section is displayed).

2.3 Finite Element Method simulations

Bidimensional finite element method (FEM) simulations of a model equivalent to the case described in subsection 2.2 (i.e. two circular electrodes with a diameter of 300 µm separated by 5 mm in a homogeneous and isotropic conductive medium of 20 mm × 20 mm) were performed with COMSOL Multiphysics 3.4 (Comsol AB, Stockholm, Sweden). In particular we employed the "Quasi-Statics, Electric" application mode of the "AC/DC Module" with a mesh of 10,440 elements. This software tool is able to compute the voltage at each point of a conductor when some parameters are specified (e.g. voltages at the boundaries and conductivities of the materials). Hence the electric field at each point is also obtained as it is the gradient of the voltage. More details about the finite element method and how it can be used for computing the electric field distribution in electroporation related problems can be found in the scientific literature [8-12].

Four conductivity models for the potato tissue were considered here: 1) constant conductivity ($\sigma(|\mathbf{E}|)$=0.3 mS/cm), 2) conductivity according to the values obtained at the "5^{th} µs" after the pulse onset (for details see section 3.1), 3) conductivity according to the values obtained at the 100^{th} µs of the pulse and 4) conductivity according to the values obtained at the end of the 400 µs pulse. In fact, as explained in section 3.1, the conductivity models at 5 µs, 100 µs and 400 µs were the sigmoid approximations of the corresponding experimental data.

The first conductivity model (i.e. constant conductivity) can be solved directly with COMSOL without further complication. On the other hand, the other three models, in which the conductivity depends on the electric field, require an iterative solving process in which the conductivity for each step of the solving procedure is defined by the field in the previous step. In this iterative process, the electric field distribution for the first step is computed under the assumption that the conductivity is uniform and equal to the conductivity of the tissue before electroporation occurs ($\sigma(|\mathbf{E}|)$=0.3 mS/cm). If in this iterative process it is modeled that the applied voltage at the electrodes is present since the first step, in some cases, the solution does not converge easily and oscillations in conductivity appear. Therefore, an alternative approach was tried here in order to facilitate convergence of the solution: the COMSOL simulation was in fact configured as a time transient simulation in which the applied voltage increased smoothly from 0 V to the final voltage (i.e. 300 V or 500 V) and then remained constant at that final value until the end of the simulation. More specifically, the voltage raise consisted of a ramp function from time 0 to time 0.1 and the simulation finished at time 2. Note that here the time points are indicated without units (e.g. seconds) as they are in fact arbitrary; time has no physical meaning

in the simulation, it is employed for facilitating the solving process. For each simulation it was verified that the solution was indeed stable and that no oscillations remained during the phase in which the applied voltage reached its final value. Finally, the electric field magnitude at each point was represented with a gray color scale according to the black content values experimentally obtained in the case of uniform field electroporation (see section 3.1).

In relation with the above indication concerning the physical meaningless of time parameter employed in the simulation, it must be noted that in the "Quasi-Statics, Electric" application mode of COMSOL Multiphysics it is required to define relative permittivity values and that we used a value of 1 for all the tissue regions. Such value has a negligible impact on the simulations due to the large scale of the artificial time scale considered here (2 seconds).

3. Results and discussion

3.1 Uniform field electroporation

Just five hours after pulse delivery, each potato tuber cylinder exposed to a 400 μs pulse with an electric field magnitude above 300 V/cm was distinctively darker than the non-treated samples. Nevertheless, in order to minimize data scattering due to differences in elapsed times after pulsation, we decided to quantify darkening (black content, K) twelve hours after pulse delivery, as described in section 2.1. The resulting quantitative data are displayed in Fig. 2. For electric field magnitudes below 200 V/cm no darkening is observed, between 200 V/cm and 600 V/cm darkening increases smoothly (observe that K is almost linear with |E| for this range) and, finally, darkening saturates for |**E**| values above 600 V/cm. The dashed trace in Fig. 2 represents the linear piecewise function that was later employed to represent the simulation data in section 3.2.

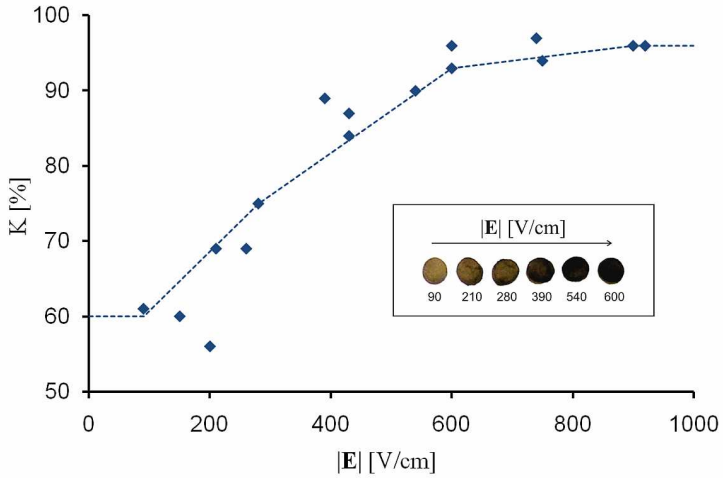

Fig. 2. The "black contents" of the electroporated potato tuber cylinders is displayed against the electric field magnitude of the pulses (see text). The insert shows some examples of electroporated potato samples 12 hours after pulse application.

(Here Fig. 2, single column)

Instant conductivity ($\sigma(t)$) during the pulse, also referred to as *dynamic conductivity*, was recorded as described in section 2.1. The original conductivity of the potato tuber before electroporation occurs, σ_0, is about 0.3 mS/cm and it was obtained by applying pulses with a magnitude below 30 V/cm, which do not cause any observable electroporation effect. On the other hand, as an example, Fig. 3.a depicts a recorded trace corresponding to a pulse of approximately 600 V/cm which shows obvious electroporation signs. In the very few first microseconds of the pulse, it can be noticed that the recorded dynamic conductivity is transiently much higher than σ_0 (e.g. >15 mS/cm against 0.3 mS/cm in Fig. 3.a). Such transitory conductivity increase is due to the cell membrane charging process (i.e. cell membranes behave as capacitances) and hence it does not constitute an indication of electroporation. As a matter of fact, this phenomenon is also observed for the 30 V/cm pulses employed for obtaining σ_0. However, when such transient ends in less than 5 μs, the conductivity stabilizes to a value that is also significantly higher than σ_0 (in Fig. 3.a $\sigma(5\mu s) \sim 2$ mS/cm) which can be explained as being the result of cell membrane permeabilization (i.e pores in the membrane). Later during the pulse, the conductivity keeps increasing at a slower pace, which would indicate an increase in the number of pores or an enlargement of the pores created in the first instants of the pulse [26].

Here we must note that when we refer to the conductivity at the 5 μs after the pulse onset we are actually referring to the minimum conductivity value that was observable after the membrane charging transient, which in all measured cases indeed occurs approximately at 5 μs after the pulse onset.

All the instant conductivity values obtained at 100 μs after the pulse onset are represented in Fig. 3.b against the electric field magnitude of the pulse. The dashed trace represents the sigmoid approximation (fitted automatically with the *Curve Fitting Toolbox* of Matlab 7.6 by The Mathworks, Inc., Natick, MA, USA) that is used later for modeling the ununiform field cases (sections 2.3 and 3.2):

$$\sigma(|\mathbf{E}|) = 3.5\, e^{-e^{-0.01(|\mathbf{E}|-250)}} + 0.3 \quad [\text{mS/cm}] \qquad (2)$$

Sigmoid functions are good models for the observed experimental behavior of tissue conductivity dependence on the electric field magnitude: constant conductivity until the electric field reaches a threshold, followed by a smooth increase in conductivity as $|\mathbf{E}|$ increases until a stable saturation level is smoothly reached. Such behavior has also been observed in other biological tissues such as *in vivo* skeletal muscle and skin [14, 27] or dense cell suspensions [28].

Fig. 3.c displays the sigmoid approximations for data obtained at 5 μs, 100 μs and 400 μs after pulse onset. It is interesting to note that data at 100 μs and at 400 μs is quite similar whereas data at 5 μs shows a lower and smoother dependency of tissue conductivity on the electric field magnitude.

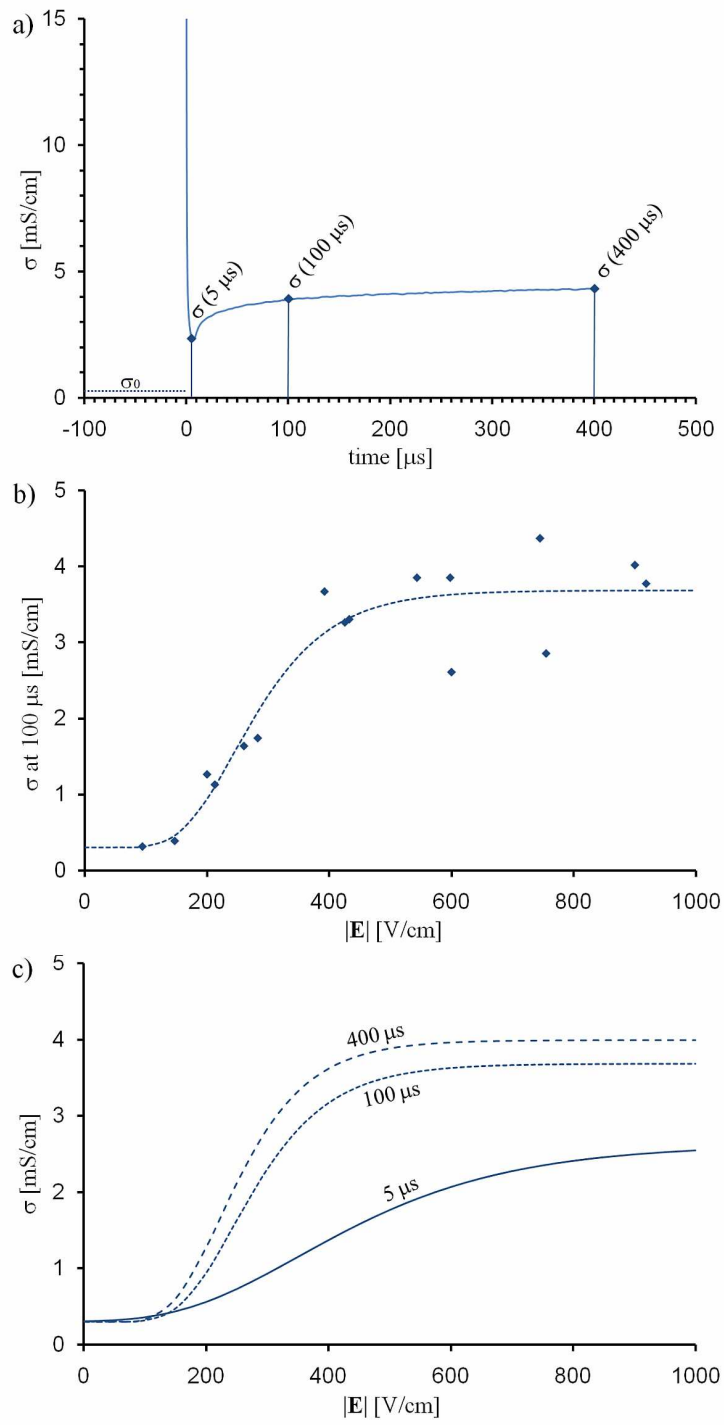

Fig. 3. Electrical conductivity measurements during the application of the pulses in the uniform field setup (Fig 1.a). (a) Example of conductivity evolution for a pulse of about 400 V/cm. (b) Conductivity values at 100 µs after pulse onset against the magnitude of the electric field. The dashed line represents the sigmoid model that was extracted from the experimental data points. (c) Obtained sigmoid models of the dependence of potato conductivity on the electric field magnitude for three different instants after pulse onset (see the text).

(Here Fig. 3, single column)

We cannot completely rule out that darkening could be caused by more indirect effects than the mere release of intracellular contents. For instance, it is plausible to assume that darkening could be induced through active release of some chemical species in response to the stress caused by the electric field damage. In a recent study by Gómez Galindo et al. with potato tubers[29], it is proposed that cell metabolic disturbance and stress caused by the electroporation pulses increases the H_2O_2 produced by cell wall-associated peroxidases which in turn reduces the permeability of the cell wall (not to be confused with the cell membrane). However, two facts strongly suggest that darkening is indeed caused by the release of intracellular contents after electroporation: 1) darkening has been identified as being the consequence of decompartmentalization caused by other physical agents different from electroporation (e.g. freezing) [23, 24]and 2) darkening is observable for field magnitudes above 200 V/cm (Fig. 2) which is the same field magnitude at which conductivity increase (i.e. cell membrane permeabilization) starts to be significant (Fig. 3.b).

Another plausible source of darkening agents could be the chemical species created by electrochemical reactions at the electrodes when the voltage pulses are applied. In particular, when aluminum electrodes are employed, it has been observed that release of Al^{3+} ions alters Ca^{2+} homeostasis in cell cultures [30]. In general, even with stainless steel or noble metal electrodes (e.g. platinum) electrochemical reactions will still occur and some chemical species will be introduced in the sample. Nevertheless, we do believe that in the case presented in the current study the impact of the electrochemically generated species is either nonexistent or negligible. Such statement is supported by the fact that the electrochemically generated species occur at the interface of the electrodes and we did not notice the corresponding darker heterogeneities. In other words, if those electrochemically generated species had had an impact on the darkening process, it would have been observed that the regions closer to the electrodes are darker than the middle regions, which we did not observe. Moreover, if it was argued that we did not see those darker areas because the chemical species were able to diffuse quickly enough, then it could be counter-argued that if diffusion was so fast then it would be impossible to obtain the well defined shapes observable in Fig. 4.a and Fig. 4.f; we would had obtained something much more blurry.

3.2 Ununiform field electroporation

As it was hypothesized, Fig. 4 shows that the predictions, made by simulating the electric field distribution, are indeed closer to the actual effects of the pulses when the dependence of the conductivity on the field is included in the models. With the aid of a digitizing software tool (Endgauge Digitizer, http://digitizer.sourceforge.net) we compared the geometrical features of the affected potato areas according to the pictures (Fig. 4.a and Fig. 4.f for pulses of 300 V and 500 V respectively) versus the darkened areas predicted by the simulations (see Table 1).

It is particularly interesting to note the improvement in treated area estimation when comparing the constant conductivity simulation and the simulation in which conductivity values at 5 μs after pulse onset are modeled: error in area estimation goes down from 33% to 2.8 % for the 300 V pulse and from 45% to 20 % for the 500 V pulse. The two other conductivity models with electric field dependence (i.e. at 100 μs and 400 μs) also produce better estimations than the constant conductivity model, however, their performance is lower than that of the 5 μs model. We

did not notice this last point in our previous conference presentation [25] because we only performed simulations with the 100 μs model. Actually, back then we assumed that the model at 100 μs would produce better results as the conductivity measured at this time point appears to be closer to the average conductivity value during the pulse than the conductivity measured at 5 μs (see Fig. 3.a). Now we do not have a robust theory for explaining why the 5 μs model seems to be better than the 100 μs model. Nevertheless we hypothesize that the fact that the conductivity dependence on |**E**| at 5 μs is smoother than the conductivity dependence at 100 μs or 400 μs may yield a larger field coverage at the beginning of the pulse. Then we hypothesize that once an outlying tissue region has experienced a large enough field to induce electroporation it may be exposed to lower field magnitudes later during the pulse, due to field redistribution, but it will still manifest the effects of the electroporation (i.e. darkening).

The conductivity models with electric field dependence not only improve treated area estimation but also seem to produce a better prediction of the shape of treated region. For instance, Fig. 4.g (constant conductivity model) shows an ellipsoidal simulated treated region whereas Fig. 4.h (conductivity model at 5 μs after pulse onset) shows an almost circular simulated treated region which looks more similar to the shape of the actual treated region (Fig. 4.f). We have tried to quantify shape distortion (see Table 1) by defining a *shape distortion factor* (*SDF*):

$$SDF = \left| \log_{10}\left(\frac{l_0}{w_0}\right) - \log_{10}\left(\frac{l}{w}\right) \right| \qquad (3)$$

where l is the length of the treated area according to the simulation (along the electrodes centers), w is the width of the treated area according to the simulation, l_0 is the length of actual treated area according to the picture and w_0 is the width of the actual treated area.

Here it is necessary to note that potato tuber is a special case of biological tissue in the sense that its extracellular conductivity is exceptionally lower than its intracellular conductivity and that induces a huge increase of conductivity when electroporation occurs (approx. ×12 in Fig. 3.b). Soft animal tissues only augment their conductivity during electroporation pulses in ×3 to ×6 factors [20, 31, 32]. Therefore, in those cases the effect of the conductivity dependence on the electric field should not have such significant consequences as the ones displayed in Fig. 4. Nevertheless, we have run a simulation (not reported here) for the muscle case and we have noticed a 30% difference in treated area estimation between the constant conductivity model and field-dependent conductivity model. Such simulation was performed with the same two needle electrode geometry as the one employed here and with a voltage between electrodes of 500 V; values for the constant conductivity model and for the sigmoid approximation for the field-dependent conductivity model were obtained from data reported in [14].

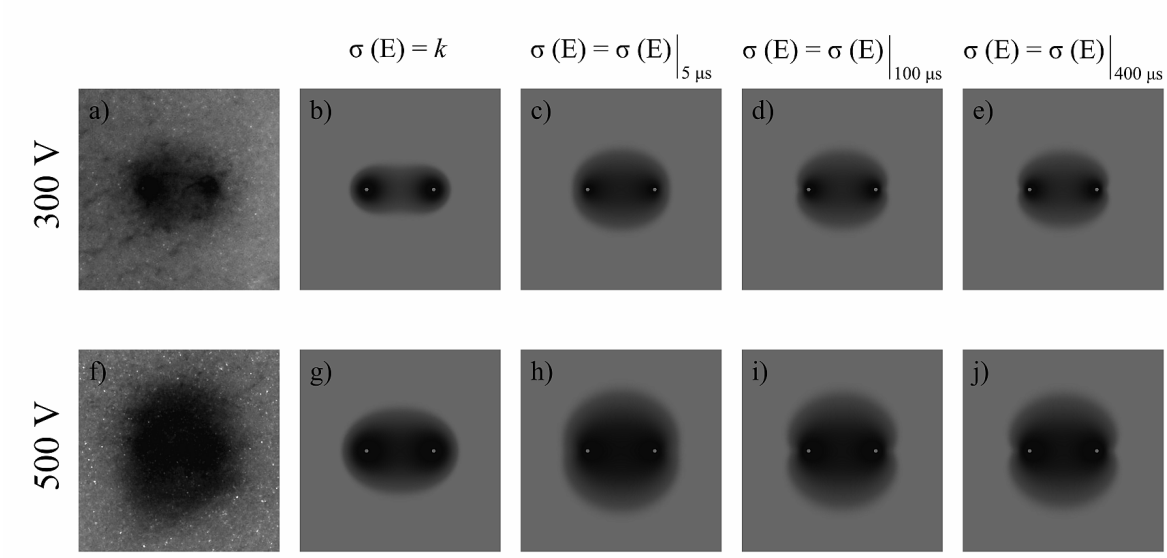

Fig. 4. Comparison of potato electroporated areas, as observed in pictures, and simulation results according to conductivity models. (a) Processed black and white picture (brightness and contrast adjustment) of a potato tuber slab 12 hours after electroporation with two parallel needles at 300 V (separation = 5mm). (b) Simulation of the previous case with a constant conductivity model. (c) Simulation of the 300 V case with a conductivity model extracted from measurements at 5 µs after pulse onset. (d) Same as (c) but at 100 µs. (e) Same as (c) but at 400 µs. (f) Processed picture from an electroporation experiment equivalent to that of (a) but with a 500 V pulse. (g) Simulation of the 500 V pulse case with a constant conductivity model. (h) Simulation of the 500 V case with a conductivity model extracted from measurements at 5 µs. (i) Same as (h) but at 100 µs. (j) Same as (h) but at 400 µs.

(Here Fig. 4 double column)

Table 1
Comparison of actual electroporated areas and simulated areas for different conductivity models. In addition, it is noted a shape distortion factor, *SDF*, for each simulation (see the text).

	picture			σ(E)=constant		σ(E) at 5 µs		σ(E) at 100 µs		σ(E) at 400 µs	
	area (mm^2)	width (mm)	length (mm)	area error (%)	*SDF*	area error (%)	*SDF*	area error (%)	*SDF*	area error (%)	*SDF*
300 V	36	6.3	7.6	-33	0.22	-2.8	0.0035	-8.5	0.012	-32	0.023
500 V	80	11.0	9.0	-45	0.21	-20	0.082	-27	0.10	-56	0.077

(Here Table 1, double column)

Finally, it is interesting to note that, as expected, darkening is not uniform all over the electroporated regions (both for actual experiments and for simulations). For instance, in Fig. 4.a. it can be observed that areas close to the electrodes (constrained within a circle of approximately 2mm in diameter) are much darker than the other electroporated areas (i.e. the ellipsoid of about 7.5 mm) and that such feature is also observable in the corresponding simulations (Figs 4.b, 4.c, 4.d and 4.e).

4. Conclusions

The present study demonstrates that prediction of the geometry of the living tissue area affected by electroporation, as assessed by numerical simulation of the electric field distribution, is significantly improved by taking into account the dependence of tissue conductivity on the electric field magnitude caused by a high-voltage pulse. For instance, in a particular case in which a potato tuber slab was electroporated with a 400 μs pulse of 300 V applied between two transversal parallel needles at a separation distance of 5 mm, the error in area estimation went down from 33% to 2.8 %. In fact, not only the affected area was better estimated but its shape (ratio between length and width) was also better reproduced by the simulation.

The obtained results seem to indicate that the predictions are better when the model for the dependence of the conductivity on the field magnitude is obtained from measurements at the first microseconds after the pulse onset (after the membrane charging transient) rather than from measurements at later instants during the pulse.

Another significant conclusion that can be extracted from the present study is that raw potato tuber is a good alternative to animal tissues for studying some specific bioelectric aspects of electroporation.

To conclude, the present study corroborates that improvements are obtained with a novel modeling methodology that was proposed recently and, in this sense, represents a significant step in our understanding of the electroporation phenomena in living tissues. Nevertheless, as it is manifested by the discrepancies between the simulation results and the experimental results, there are still some unknown aspects that are not taken into account by the modeling methodology. Therefore, further research is still needed before reaching a final description of the tissue electroporation processes.

5. Acknowledgements

This work was supported in part by U.S. National Institutes of Health (NIH) under Grant NIH R01 RR018961. This work was also supported in part by grants from: CNRS, Institute of cancerology Gustave-Roussy, University Paris Sud, INCa (National Institute of Cancer, France – contract number 07/3D1616/Doc-54-3/NG-NC) and French National Agency (ANR) through Nanoscience and Nanotechnology program (Nanopulsebiochip n° ANR-08-NANO-024).
AI's research is currently supported by a Ramón y Cajal fellowship from the Spanish Ministry for Science and Innovation.

References

[1] L. M. Mir, Therapeutic perspectives of in vivo cell electropermeabilization, Bioelectrochemistry 53 (2001) 1-10.

[2] M. J. Jaroszeski, R. Heller, R. Gilbert, Electrochemotherapy, Electrogenetherapy, and Transdermal Drug Delivery, Humana Press, Totowa, New Jersey, 2000.

[3] D. A. Dean, Nonviral gene transfer to skeletal, smooth, and cardiac muscle in living animals, Am. J. Physiol. Cell. Physiol. 289 (2005) C233-45.

[4] A. Gothelf, L. M. Mir, J. Gehl, Electrochemotherapy: results of cancer treatment using enhanced delivery of bleomycin by electroporation, Cancer Treat. Rev. 29 (2003) 371-387.

[5] R. V. Davalos, I. L. Mir, B. Rubinsky, Tissue ablation with irreversible electroporation, Ann. Biomed. Eng. 33 (2005) 223-231.

[6] B. Al-Sakere, et al, Tumor ablation with irreversible electroporation, PLoS One 2 (2007) e1135.

[7] G. Onik, P. Mikus, B. Rubinsky, Irreversible electroporation: implications for prostate ablation, Technol. Cancer. Res. Treat. 6 (2007) 295-300.

[8] D. Miklavcic, et al, The importance of electric field distribution for effective in vivo electroporation of tissues, Biophys. J. 74 (1998) 2152-2158.

[9] K. Sugibayashi, et al, Electric field analysis on the improved skin concentration of benzoate by electroporation, Int. J. Pharm. 219 (2001) 107-112.

[10] S. B. Dev, D. Dhar, W. Krassowska, Electric field of a six-needle array electrode used in drug and DNA delivery in vivo: analytical versus numerical solution, IEEE Trans. Biomed. Eng. 50 (2003) 1296-1300.

[11] J. F. Edd, et al, In vivo results of a new focal tissue ablation technique: irreversible electroporation, IEEE Trans. Biomed. Eng. 53 (2006) 1409-1415.

[12] D. Miklavcic, et al, A validated model of in vivo electric field distribution in tissues for electrochemotherapy and for DNA electrotransfer for gene therapy, Biochim. Biophys. Acta 1523 (2000) 73-83.

[13] D. Sel, et al, Sequential finite element model of tissue electropermeabilization, IEEE Trans. Biomed. Eng. 52 (2005) 816-827.

[14] A. Ivorra, et al, Use of conductive gels for electric field homogenization increases the antitumor efficacy of electroporation therapies, Phys. Med. Biol. 53 (2008) 6605-6618.

[15] R. C. Lee, D. Zhang, J. Hannig, Biophysical injury mechanisms in electrical shock trauma, Annu. Rev. Biomed. Eng. 2 (2000) 477-509.

[16] R. V. Davalos, et al, Electrical impedance tomography for imaging tissue electroporation, IEEE Trans. Biomed. Eng. 51 (2004) 761-767.

[17] U. Pliquett, et al, Electroporation of subcutaneous mouse tumors by rectangular and trapezium high voltage pulses, Bioelectrochemistry 62 (2004) 83-93.

[18] S. V. Belov, Effect of high-frequency current parameters on tissue coagulation, Med. Tekh. (4) (1978) 44-47.

[19] A. Ivorra, B. Rubinsky, In vivo electrical impedance measurements during and after electroporation of rat liver, Bioelectrochemistry 70 (2007) 287-295.

[20] A. Ivorra, et al, In vivo electrical conductivity measurements during and after tumor electroporation: conductivity changes reflect the treatment outcome, Phys. Med. Biol. 54 (2009) 5949-5963.

[21] R. C. Lee, et al, Surfactant-induced sealing of electropermeabilized skeletal muscle membranes in vivo, Proc. Natl. Acad. Sci. U. S. A. 89 (1992) 4524-4528.

[22] W. M. S. Russell, *The Principles of Humane Experimental Technique.* London: Methuen & Co, 1959,

[23] I. N. A. Ashie, B. K. Simpson, Application of high hydrostatic pressure to control enzyme related fresh seafood texture deterioration, Food Res. Int. 29 (1996) 569-575.

[24] J. F. Edd, et al, Imaging cryosurgery with EIT: tracking the ice front and post-thaw tissue viability, Physiol. Meas. 29 (2008) 899-912.

[25] A. Ivorra, L. M. Mir, B. Rubinsky, Electric Field Redistribution due to Conductivity Changes during Tissue Electroporation: Experiments with a Simple Vegetal Model, IFMBE Proceedings 25 (2009) 59-62.

[26] K. A. DeBruin, W. Krassowska, Modeling electroporation in a single cell. I. Effects Of field strength and rest potential, Biophys. J. 77 (1999) 1213-1224.

[27] N. Pavselj, et al, The course of tissue permeabilization studied on a mathematical model of a subcutaneous tumor in small animals, IEEE Trans. Biomed. Eng. 52 (2005) 1373-1381.

[28] K. Kinosita Jr, T. Y. Tsong, Voltage-induced conductance in human erythrocyte membranes, Biochim. Biophys. Acta 554 (1979) 479-497.

[29] F. G. Galindo, et al, Pulsed electric field reduces the permeability of potato cell wall, Bioelectromagnetics 29 (2008) 296-301.

[30] J. W. Loomis-Husselbee, et al, Electroporation can cause artefacts due to solubilization of cations from the electrode plates. Aluminum ions enhance conversion of inositol 1,3,4,5-tetrakisphosphate into inositol 1,4,5-trisphosphate in electroporated L1210 cells, Biochem. J. 277 (Pt 3) (1991) 883-885.

[31] A. Ivorra, B. Rubinsky, In vivo electrical impedance measurements during and after electroporation of rat liver, Bioelectrochemistry 70 (2007) 287-295.

[32] D. Cukjati, et al, Real time electroporation control for accurate and safe in vivo non-viral gene therapy, Bioelectrochemistry 70 (2007) 501-507.